ACS APPLIED ENERGY MATERIALS
Cite This: ACS Appl. Energy Mater. 2018, 1, 1077−1082
Article
www.acsaem.org

Fabrication of Back-Contact Electrodes Using Modified Natural Lithography

Askhat N. Jumabekov,[†,∥] Julian A. Lloyd,[‡,∥] Dorota M. Bacal,[§] Udo Bach,*[,§] and Anthony S. R. Chesman*[,†]

[†]CSIRO Manufacturing, Clayton, Victoria 3168, Australia

[‡]Department of Materials Science & Engineering and [§]Department of Chemical Engineering, Monash University, Clayton, Victoria 3168, Australia

Supporting Information

ABSTRACT: The fabrication of back-contact electrodes with micron-sized features by microsphere lithography is implemented via a modified "natural lithography" approach. The solution-based assembly of microsphere beads on a substrate occurs via the electrostatic attraction between the molecular monolayer-functionalized substrate and the micron-sized polystyrene microbeads with carboxyl surface groups. Through a modification of the original "natural lithography" method, the density of the microbeads used as a lithographic mask can be increased 5-fold. The resulting back-contact electrodes are used for the fabrication of perovskite solar cell devices and the examination of their potential. Devices with electrodes fabricated using a modified "natural lithography" approach showed a 3.5-fold increase in performance compared to the devices with electrodes made using the original method.

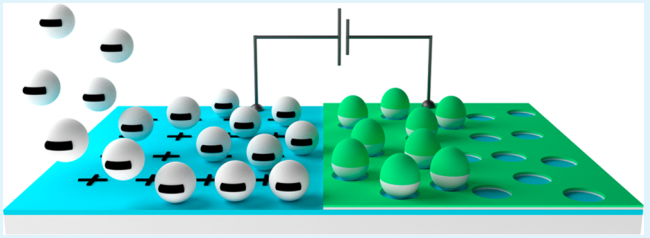

KEYWORDS: *lithography, microbeads, microsphere lithography, back-contact electrodes, perovskite, solar cells*

1. INTRODUCTION

Back-contact electrodes (BCEs) are utilized in a wide variety of applications, including electrochemical sensors for analytical chemistry[1−3] and biochemical[4−8] studies, field effect transistors,[9,10] and high-performance optoelectronic devices (e.g., light-emitting diodes,[11] photodetectors,[12,13] and solar cells[14−17]). Despite their broad application, the manufacturing cost of BCEs remains high, as to date, they have been fabricated using high-cost methods, like optical, electron-beam and X-ray lithography. However, an alternative lithographic technique, microsphere lithography (ML), permits facile, readily scalable, and cost-effective patterning[18,19] and has already been applied to electrochromics,[20] photonics,[21,22] plasmonics,[23−26] photocatalysis,[27] and various electrode fabrications.[28−31] Therefore, extending the application of ML to BCE production potentially confers considerable advantages over conventional lithographic techniques and presents a pathway to large-scale production.

Traditionally, the contacts (anode and cathode) of BCEs are arranged into an interdigitated array on a planar substrate, as shown in Figure 1a. While the fabrication of interdigitated electrodes (IDEs) via a top-down approach, such as photolithography or electron-beam lithography, is well established, it is yet to be achieved by ML. Recently, Jumabekov et al.[32] reported a novel BCE architecture, in which one-half of the interdigitated electrode is deposited onto a continuous layer of the other electrode, as shown in Figure 1b. The finger-type design for the "top" electrode (cathode in Figure 1b) allows for a partially exposed "bottom" electrode (anode in Figure 1b),

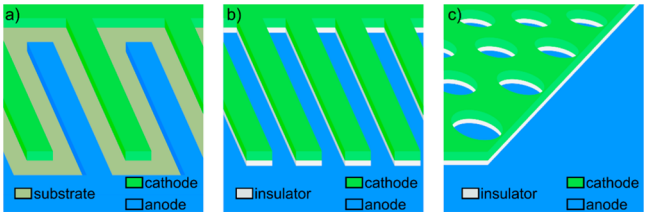

Figure 1. Designs of back-contact electrodes (BCEs). (a) Interdigitated electrodes (IDEs). (b) Quasi-interdigitated electrodes (QIDEs). (c) Quasi-integrated electrodes (QIEs).

with a thin layer of insulator separating the two electrodes and preventing contact, which would cause short-circuiting. BCEs with such a design are referred to as quasi-interdigitated electrodes (QIDEs).[32]

A modification of this design, in which the finger-like shape of the cathode is replaced by a grid-type electrode as shown in Figure 1c (hereon quasi-integrated electrodes (QIEs)), presents two major advantages. First, minor QIDE fabrication errors result in electrode fingers that are either broken or entirely disconnected from the base, which isolate these regions from charge collection. In contrast, the QIE is less vulnerable to local defects due to redundancy in the interconnections, making QIEs more robust and defect tolerant. Second, the morphology

Received: December 1, 2017
Accepted: February 20, 2018
Published: February 20, 2018

DOI: 10.1021/acsaem.7b00213
ACS Appl. Energy Mater. 2018, 1, 1077−1082

Scheme 1. Fabrication Process for QIEs via Modified "Natural Lithography"[a]

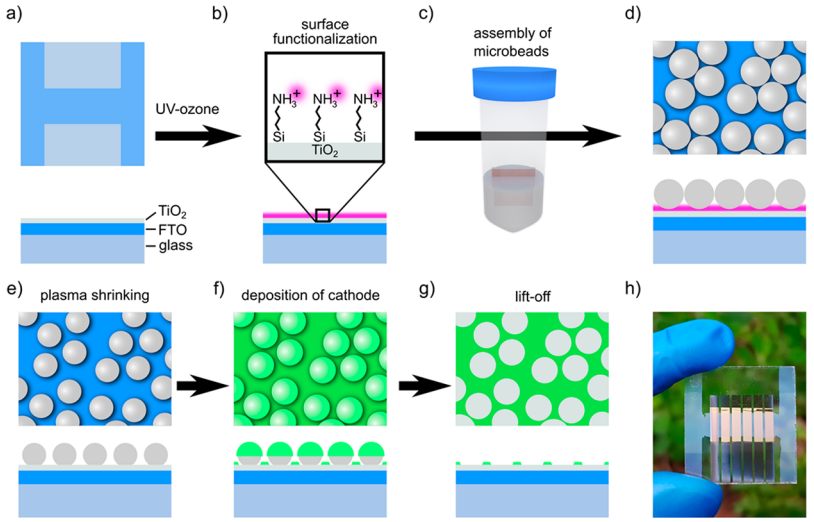

[a](a) Patterned glass/FTO/TiO_2 anodes. (b) Surface functionalization of the anode's surface with APTES SAM. (c) Assembly of a monolayer of polystyrene microbeads on the anode. (d) Monolayer of polystyrene microbeads assembled on the surface of anode. (e) SLM on the anode. (f) The anode with SLM after deposition of a cathode layer. (g) A QIE after lift-off. (h) Photographic image of a QIEs.

of the top electrode in QIEs offers the possibility of using ML for their fabrication.

In ML, the sacrificial lithographic mask (SLM) is formed from a monolayer of monodisperse polymer microbeads deposited onto a substrate (bottom-up approach). The coverage and packing of the monolayer of microbeads are of significant importance, as they determine the shape, size, and quality of the resulting mask. There are a number of different methods for depositing a monolayer of polymer microbeads on a substrate: spin-coating,[33] electrophoretic deposition,[34] and various self-assembly methods (chemical or electrochemical,[35−37] template-guided,[38] controlled evaporation,[39] lift-up,[40] Langmuir−Blodgett technique[41]). As each of these methods possess certain requirements for the type of substrate, namely, its surface (planar or/and structured), plasticity (rigid or/and flexible), electrical property (conducting or/and insulating), wettability (hydrophilic or/and hydrophobic), and deposition conditions (temperature, humidity, pressure of the buffer atmosphere), it is preferable to explore methods that are largely independent of these constraints, affording facile, large-area, and cost-effective fabrication of BCEs.

In this regard, so-called "natural lithography",[35,42−44] a type of electrochemical self-organization method,[36] is a subcategory of ML that largely fulfils these criteria. First reported by Deckman et al.,[35] SLM formation with "natural lithography" relied on the electrostatic attraction between negatively charged polystyrene microbeads (~0.9 μm) and a positively charged Al_2O_3 substrate at pH 5.0.[31] However, the coverage of the substrate surface with microbeads is sensitive to the pH value of the electrolyte (usually between 5 to 6) in which the microbeads are suspended (colloidal solution). If a substrate's surface reaches or is around its point of zero charge (pzc) condition at the pH value of the colloidal solution (e.g., TiO_2 and SnO_2 have pzc values of around pH 6 and 5.5, respectively),[45,46] coverage is insufficient due to the negligible electrostatic attraction between the substrate and the negatively charged microbeads.[35] This makes fabrication of good quality SLMs using "natural lithography" on such substrates challenging. Herein, we demonstrate that this limitation in the original "natural lithography" method is overcome effectively by using self-assembled monolayers (SAMs) to functionalize the surface of the substrates to boost the electrostatic attraction and deposition of denser monolayer of microbeads on substrates. A remarkable enhancement in coverage was obtained via modified "natural lithography" as opposed to the original protocol. Using modified "natural lithography", we successfully fabricated novel QIEs and demonstrated the potential of this concept by using QIEs as BCEs in perovskite solar cells (PSCs).

2. RESULTS AND DISCUSSION

We started the fabrication of QIEs by preparing the anodes; a thin layer of TiO_2 (~30 nm) was deposited via spray pyrolysis onto 25 × 25 mm prepatterned fluorine-doped tin oxide (FTO) coated glass substrates (Scheme 1a). Spray pyrolysis yields a conformal and high-quality crystalline TiO_2 layer, a standard anode layer for many optoelectronic devices.[16,31,47] Freshly made anodes were then functionalized with (3-aminopropyl)triethoxysilane (APTES). Due to the hydrolysis and subsequent condensation of APTES onto OH-bearing TiO_2 substrates, a SAM of APTES formed on the substrates (Scheme 1b).[48] In the next step, the functionalized substrates were immersed into a colloidal solution for ~8 h at room temperature in order to deposit a monolayer of microbeads (modified "natural lithography") (Scheme 1c). The colloidal solution with a pH value of 5.5 contains monodisperse 1-μm-sized polystyrene microbeads with surface carboxyl groups.

In order to test the efficacy of modified "natural lithography" in comparison to the original protocol,[35] we performed additional studies, in which substrates with a bare TiO_2 layer (glass/FTO/TiO_2 substrates without APTES functionalization) were also immersed into the same colloidal solution under similar conditions to replicate the original method. A comparison revealed that modified "natural lithography" yields a higher deposition rate of polystyrene microbeads (Figure 2a). The APTES-functionalized substrate appears to be more opaque than the nonfunctionalized substrate, indicating a more densely deposited monolayer of polystyrene microbeads in the former. Figure 2b,c shows the corresponding photo-

DOI: 10.1021/acsaem.7b00213
ACS Appl. Energy Mater. 2018, 1, 1077−1082

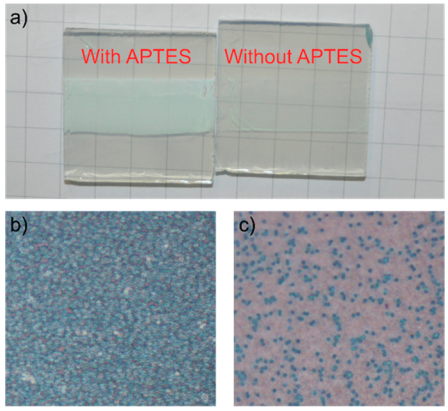

Figure 2. Anodes with SLM of microbeads. (a) Photographic image of glass/FTO/TiO_2 substrates with SLM formed via modified (left) and unmodified (right) "natural lithography" methods. Optical micrographs of glass/FTO/TiO_2 substrates with SLM formed by (b) modified and (c) unmodified "natural lithography" methods (magnification: 50×).

micrographs that confirm much denser deposition of polystyrene microbeads.

The disparity between the deposition rates of the polymer microbeads on these two substrates can be rationalized as follows: at a pH value of 5.5, the surface of the microbeads is negatively charged due to deprotonation of carboxyl groups (see Figure S1 in the Supporting Information);[31,49] the surface of an APTES-functionalized TiO_2 substrate is positively charged due to protonation of amine groups of the APTES SAM,[50,51] and the surface of a neat TiO_2 substrate is close to its pzc condition at a pH of 5.5, thus being only weakly positively charged.[45,46] This results in a higher electrostatic attraction between the microbeads and the APTES-functionalized TiO_2 than for the bare TiO_2. Hence, the deposition rate of microbeads on the APTES-functionalized substrate is higher than the one without any APTES SAM functionalization, ultimately resulting in a denser coverage of microbeads.

In Figure 3a, a micrograph obtained using scanning electron microscopy (SEM) shows the arrangement of as-deposited polystyrene microbeads on the surface of an APTES-functionalized glass/FTO/TiO_2 substrate. The micrograph reveals that the arrangement of the microbeads is relatively dense but somewhat clustered and irregular in nature. In order to complete the microfabrication of the SLM, the substrates were heat treated on a hot plate at 110 °C for 5 min in order to firmly fix the positions of the microbeads to the substrate by slightly melting the base of the microbeads to the substrate, thus preventing the microbeads from local migration (see Figure S2 in the Supporting Information). The substrate was then subjected to an air plasma treatment in order to shrink the size of the microbeads and separate them from each other (Scheme 1e). Figure 3b shows a micrograph of successful SLM deposition on a glass/FTO/TiO_2 anode substrate, i.e., isolated and shrunk submicron (between 600 and 900 nm) polymer beads.

In the next step, an Al_2O_3 insulator (120 nm), an Al wetting layer (30 nm), and a NiCo alloy (50 nm, 1:1 ratio) were sequentially evaporated onto the substrates (Scheme 1f) using an electron-beam evaporator to form the cathode layer (see the energy dispersive spectroscopy (EDS) map in Figure S3 in the Supporting Information). The SLM was then removed by washing the substrates in toluene or tetrahydrofuran (THF) to

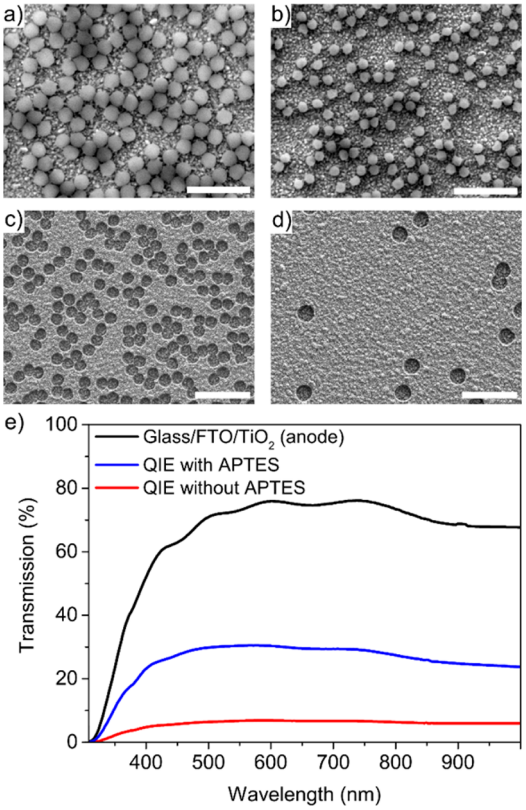

Figure 3. Modified "natural lithography" vs original "natural lithography". (a) Polystyrene microbeads on the surface of an APTES-functionalized glass/FTO/TiO_2 substrate. (b) SLM on a glass/FTO/TiO_2 substrate. (c) A QIE with APTES functionalization. (d) A QIE without APTES functionalization. (e) UV−vis−NIR transmission spectra of a neat anode, and QIEs with and without APTES functionalization. All scale bars are 4 μm.

expose the bottom TiO_2 anode layer (Scheme 1g). Figure 3c,d shows SEM micrographs of the active area (anode and cathode regions) of electrodes for modified and unmodified "natural lithography" methods.

In order to estimate the area of the exposed anode (circles in Figures 3c,d) we performed UV−vis−NIR transmission measurements on QIEs with and without APTES functionalization (Figure 3e). The reference plain glass/FTO/TiO_2 substrate (neat anode) shows an ∼75% transmission value for the majority of the visible spectrum, while the complete QIEs with and without APTES functionalization demonstrate around 28 and 6% over the same region, respectively. This indicates that relative to the reference glass/FTO/TiO_2 substrate, the overall anode area for QIEs with and without APTES functionalization is around 40% and 9%, respectively (see Figure S4a in the Supporting Information). Hence, a relative gain in SLM coverage through modified "natural lithography" can be estimated from the UV−vis−NIR transmission measurements by calculating the ratio of the spectra for QIEs with and without APTES functionalization (see Figure S4b in the Supporting Information). This yields a value 4.4 ± 0.5 for the relative increase in transmission across the 300−1000 nm wavelength range, revealing an almost 5-fold increase in surface coverage of the anode with polymer microbeads with an APTES-functionalized substrate.

The electrode fabrication process is completed by heat treating the QIEs at 300 °C for 15 min in an ambient

DOI: 10.1021/acsaem.7b00213
ACS Appl. Energy Mater. 2018, 1, 1077−1082

atmosphere in order to form oxide shells ($NiCoO_x$ and Al_2O_3) around the exposed metallic components of the cathode.[32] Here, NiCo with its $NiCoO_x$ layer forms the cathode of the QIEs, with Ni-doped CoO_x previously being shown to be an efficient HTL in perovskite solar cells.[52,53] The work function and ionization potential of NiCo and $NiCoO_x$, respectively, were measured with photoelectron spectroscopy in air (PESA), with the latter found to be a suitable hole acceptor for methylammonium lead iodide ($CH_3NH_3PbI_3$, $MAPbI_3$) due to their desirable band alignment (see Figure S5 in Supporting Information). A photographic image of a complete QIE is shown in Scheme 1h. A more detailed description of the fabrication process is given in the Supporting Information.

The QIEs, both made using modified and unmodified "natural lithography" methods, were incorporated into back-contact perovskite solar cells (PSC) in order to examine the potential of the new concept as well as the efficacy of the new protocol over the original process. In this lateral p-i-n device structure, the perovskite is the i-type photoabsorber, while the $NiCo_x$ and TiO_2 act as the p-type and n-type charge transport layers, respectively. Al/NiCo and FTO are the contacts. The ETL and HTL and their respective contacts are separated by the insulating Al_2O_3 layer (see Figure 1c). A thin layer of the perovskite was deposited via spin-coating a perovskite precursor solution onto freshly made QIEs in an inert atmosphere with subsequent annealing at 100 °C for 10 min. Figure 4a shows a cross section SEM micrograph of a QIE-based back-contact PSC, with Figure 4b partially color-coding the different functional layers of the back-contact PSC device in a high-magnification cross section SEM micrograph (the section in Figure 4a enclosed with a red rectangle).

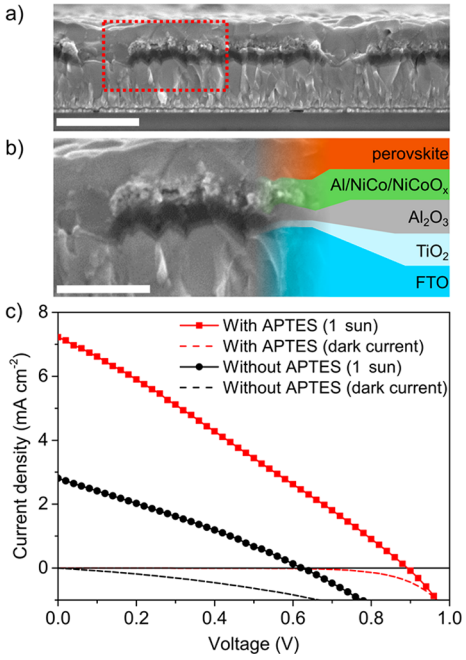

Figure 4. Back-contact PSCs. (a) Cross section SEM micrograph of a PSC (low magnification, scale bar is 1 μm). (b) Color-coded cross section SEM micrograph of a PSC (high magnification, scale bar is 500 nm). (c) $J-V$ characteristics (reverse scans) of QIE-based PSCs with electrodes made via modified and unmodified protocols for "natural lithography".

$J-V$ characteristics of the devices were recorded in the dark and under simulated sunlight (AM1.5G; 1000 W m^{-2}) to evaluate the performance of the solar cells. The cell with the electrode prepared using modified "natural lithography" shows a better rectifying $J-V$ curve in the dark, indicating better diode behavior than that of the reference cell prepared using the original "natural lithography" protocol (Figure 4c). Under illumination, both devices exhibited a photovoltaic effect, with the device with APTES functionalization exhibiting much better solar cell performance. The $J-V$ curve under illumination for the reference device shows a power conversion efficiency (PCE) value of 0.5% with 2.8 mA cm^{-2}, 0.62 V, and 29% for the short-circuit current density (J_{SC}), open-circuit voltage (V_{OC}) and fill factor, respectively, while the device prepared using modified "natural lithography" shows significantly improved performance, with a PCE value of 1.75% and J_{SC}, V_{OC}, and fill factor values being 7.2 mA cm^{-2}, 0.9 V and 27%, respectively (see Figure S6 in the Supporting Information). Examination of the resistances of the devices also reveals an improvement with the use of ML, with a comparison of the device fabricated with modified "natural lithography" to the reference device showing a decrease in the R_S from 28.0 to 18.5 $\Omega\cdot cm^2$ and an increase in the R_{SH} from 1.16 to 16.35 $k\Omega\cdot cm^2$, respectively. The 3.5-fold increase in PCE for the PSC prepared using modified "natural lithography" can be attributed to a more balanced contact between the anode and cathode surfaces and perovskite photoabsorber layer, which facilitates enhanced charge injection at the electrode/perovskite interfaces and ultimately improves the photovoltaic performance of the device.

3. CONCLUSIONS

We have presented an implementation of a facile ML technique through the modification of "natural lithography" to prepare low-cost BCEs. We demonstrate that functionalizing TiO_2 substrates with APTES SAMs significantly enhances the electrostatic attraction between the glass/FTO/TiO_2 anode and the polystyrene colloidal microbeads with carboxyl groups on their surfaces. Hence, this provides a way to effectively overcome the limitation of the original "natural lithography" method, in which the formation of the SLM is hindered due to insufficient electrostatic attraction between the substrate and microbeads when the pzc value of the substrate coincides with the pH value of the colloidal microbeads solution. We anticipate that further fine-tuning of the modified "natural lithography" method, for instance, through employing SAMs that can induce an even higher positive charge at the substrates' surface, can result in the formation of a monolayer of microbeads, as well as SLMs, with higher order. This offers a versatile approach to designing QIEs with the desired anode-to-cathode surface ratio by simply choosing SAMs with the appropriate functional groups. Additionally, novel BCEs with a new quasi-integrated design are robust and have a higher intrinsic defect tolerance compare to common finger-type interdigitated[1−17] or quasi-interdigitated[32] BCEs. This, combined with an inexpensive and facile fabrication method, offers immense potential for large-scale, and potentially roll-to-roll, industrial production of BCEs. As a proof of concept, we demonstrated the use of QIEs as an electrode for PSCs with a back-contact design. However, we expect this general concept to be adaptable to a wide range of applications.

DOI: 10.1021/acsaem.7b00213
ACS Appl. Energy Mater. 2018, 1, 1077−1082

■ ASSOCIATED CONTENT

Supporting Information

The Supporting Information is available free of charge on the ACS Publications website at DOI: 10.1021/acsaem.7b00213.

Experimental section; zeta potential−pH graph; SEM micrograph of SLM on anode; energy dispersive spectroscopy (EDS) map of a QIE; analysis of UV−vis−NIR spectra; PESA measurements; *J*−*V* characteristics (PDF)

■ AUTHOR INFORMATION

Corresponding Authors

*E-mail: anthony.chesman@csiro.au (A.S.R.C.)
*E-mail: udo.bach@monash.edu (U.B.)

ORCID

Askhat N. Jumabekov: 0000-0003-0051-9542
Udo Bach: 0000-0003-2922-4959
Anthony S. R. Chesman: 0000-0002-1807-4468

Author Contributions

‖A.N.J. and J.A.L. contributed equally to this work.

Author Contributions

The manuscript was written through contributions of all authors. All authors have given approval to the final version of the manuscript.

Funding

This work was funded through CSIRO Manufacturing as part of an Office of the Chief Executive Postdoctoral Fellowship (A.N.J.). This work was financially supported by the Australian Government through the Australian Renewable Energy Agency and the Australian Centre for Advanced Photovoltaics. We gratefully acknowledge financial support from the Australian Research Council (CE170100026, FT150100450, and DP160104575).

Notes

The authors declare no competing financial interest.

■ ACKNOWLEDGMENTS

This work was performed in part at the Melbourne Centre for Nanofabrication (MCN) in the Victorian Node of the Australian National Fabrication Facility (ANFF). The authors thank Mr. Mark Greaves from CSIRO Manufacturing for his help with SEM imaging.

■ ABBREVIATIONS

BCE, back-contact electrode
ML, microsphere lithography
IDE, interdigitated electrode
QIDE, quasi-interdigitated electrode
QIE, quasi-integrated electrode
SLM, sacrificial lithographic mask
pzc, point of zero charge
SAM, self-assembled monolayer
PSC, perovskite solar cell
FTO, fluorine-doped tin oxide
APTES, (3-aminopropyl)triethoxysilane
SEM, scanning electron microscopy
EDS, energy dispersive spectroscopy
PCE, power conversion efficiency

■ REFERENCES

(1) Takahashi, M.; Morita, M.; Niwa, O.; Tabei, H. Highly Sensitive High-Performance Liquid Chromatography Detection of Catecholamine with Interdigitated Array Microelectrodes. *J. Electroanal. Chem.* **1992**, *335*, 253−263.
(2) Tabei, H.; Takahashi, M.; Hoshino, S.; Niwa, O.; Horiuchi, T. Subfemtomole Detection of Catecholamine with Interdigitated Array Carbon Microelectrodes in HPLC. *Anal. Chem.* **1994**, *66*, 3500−3502.
(3) Cohen, A. E.; Kunz, R. R. Large-Area Interdigitated Array Microelectrodes for Electrochemical Sensing. *Sens. Actuators, B* **2000**, *62*, 23−29.
(4) Niwa, O.; Xu, Y.; Halsall, H. B.; Heineman, W. R. Small-Volume Voltammetric Detection of 4-Aminophenol with Interdigitated Array Electrodes and Its Application to Electrochemical Enzyme Immunoassay. *Anal. Chem.* **1993**, *65*, 1559−1563.
(5) Yang, L.; Li, Y.; Erf, G. F. Interdigitated Array Microelectrode-Based Electrochemical Impedance Immunosensor for Detection of Escherichia coli O157:H7. *Anal. Chem.* **2004**, *76*, 1107−1113.
(6) Thomas, J. H.; Kim, S. K.; Hesketh, P. J.; Halsall, H. B.; Heineman, W. R. Microbead-Based Electrochemical Immunoassay with Interdigitated Array Electrodes. *Anal. Biochem.* **2004**, *328*, 113−122.
(7) Ohno, R.; Ohnuki, H.; Wang, H.; Yokoyama, T.; Endo, H.; Tsuya, D.; Izumi, M. Electrochemical Impedance Spectroscopy Biosensor with Interdigitated electrode for Detection of human immunoglobulin A. *Biosens. Bioelectron.* **2013**, *40*, 422−426.
(8) Huang, C.-W.; Lu, M. S.-C. Electrochemical Detection of the Neurotransmitter Dopamine by Nanoimprinted Interdigitated Electrodes and a CMOS Circuit with Enhanced Collection Efficiency. *IEEE Sens. J.* **2011**, *11*, 1826−1831.
(9) Liscio, A.; Orgiu, E.; Mativetsky, J. M.; Palermo, V.; Samorì, P. Bottom-Up Fabricated Asymmetric Electrodes for Organic Electronics. *Adv. Mater.* **2010**, *22*, 5018−5023.
(10) Chin, X. Y.; Cortecchia, D.; Yin, J.; Bruno, A.; Soci, C. Lead Iodide Perovskite Light-Emitting Field-Effect Transistor. *Nat. Commun.* **2015**, *6*, 7383.
(11) Pei, Q.; Yu, G.; Zhang, C.; Yang, Y.; Heeger, A. J. Polymer light-emitting electrochemical cells. *Science* **1995**, *269*, 1086−1088.
(12) Brendel, M.; Helbling, M.; Knigge, A.; Brunner, F.; Weyers, M. Solar-Blind AlGaN MSM Photodetectors with 24% External Quantum Efficiency at 0 V. *Electron. Lett.* **2015**, *51*, 1598−1600.
(13) Saidaminov, M. I.; Adinolfi, V.; Comin, R.; Abdelhady, A. L.; Peng, W.; Dursun, I.; Yuan, M.; Hoogland, S.; Sargent, E. H.; Bakr, O. M. Planar-Integrated Single-Crystalline Perovskite Photodetectors. *Nat. Commun.* **2015**, *6*, 8724.
(14) Wang, W.; Liu, F.; Man Lau, C.; Wang, L.; Yang, G.; Zheng, D.; Li, Z. Field-Effect $BaTiO_3$-Si Solar Cells. *Appl. Phys. Lett.* **2014**, *104*, 123901.
(15) Xiao, Z.; Yuan, Y.; Shao, Y.; Wang, Q.; Dong, Q.; Bi, C.; Sharma, P.; Gruverman, A.; Huang, J. Giant Switchable Photovoltaic Effect in Organometal Trihalide Perovskite Devices. *Nat. Mater.* **2015**, *14*, 193−198.
(16) Pazos-Outón, L. M.; Szumilo, M.; Lamboll, R.; Richter, J. M.; Crespo-Quesada, M.; Abdi-Jalebi, M.; Beeson, H. J.; Vrućinić, M.; Alsari, M.; Snaith, H. J.; et al. Photon Recycling in Lead Iodide Perovskite Solar Cells. *Science* **2016**, *351*, 1430−1433.
(17) Lin, X.; Jumabekov, A. N.; Lal, N. N.; Pascoe, A. R.; Gómez, D. E.; Duffy, N. W.; Chesman, A. S. R.; Sears, K.; Fournier, M.; Zhang, Y.; Bao, Q.; Cheng, Y.; Spiccia, L.; Bach, U. Dipole-Field-Assisted Charge Extraction in Metal-Perovskite-Metal Back-Contact Solar Cells. *Nat. Commun.* **2017**, *8*, 613.
(18) Hulteen, J. C.; Van Duyne, R. P. Nanosphere Lithography: A Materials General Fabrication Process for Periodic Particle Array Surfaces. *J. Vac. Sci. Technol., A* **1995**, *13*, 1553−1558.
(19) Acikgoz, C.; Hempenius, M. A.; Huskens, J.; Vancso, G. J. Polymers in Conventional and Alternative Lithography for the Fabrication of Nanostructures. *Eur. Polym. J.* **2011**, *47*, 2033−2052.
(20) Xia, X. H.; Tu, J. P.; Zhang, J.; Xiang, J. Y.; Wang, X. L.; Zhao, X. B. Cobalt Oxide Ordered Bowl-Like Array Films Prepared by

DOI: 10.1021/acsaem.7b00213
ACS Appl. Energy Mater. 2018, 1, 1077−1082

Electrodeposition through Monolayer Polystyrene Sphere Template and Electrochromic Properties. *ACS Appl. Mater. Interfaces* **2010**, *2*, 186−192.
(21) Rogach, A.; Susha, A.; Caruso, F.; Sukhorukov, G.; Kornowski, A.; Kershaw, S.; Möhwald, H.; Eychmüller, A.; Weller, H. Nano- and Microengineering: Three-Dimensional Colloidal Photonic Crystals Prepared from Submicrometer-Sized Polystyrene Latex Spheres Pre-Coated with Luminescent Polyelectrolyte/Nanocrystal Shells. *Adv. Mater.* **2000**, *12*, 333−337.
(22) Zhou, Z.; Zhao, X. S. Flow-Controlled Vertical Deposition Method for the Fabrication of Photonic Crystals. *Langmuir* **2004**, *20*, 1524−1256.
(23) Ng, W. N.; Leung, C. H.; Lai, P. T.; Choi, H. W. Photonic Crystal Light-Emitting Diodes Fabricated by Microsphere Lithography. *Nanotechnology* **2008**, *19*, 255302.
(24) Ungureanu, S.; Kolaric, B.; Chen, J.; Hillenbrand, R.; Vallée, R. A. L. Far-Field Disentanglement of Modes in Hybrid Plasmonic-Photonic Crystals by Fluorescence Nano-Reporters. *Nanophotonics* **2013**, *2*, 173−185.
(25) Lohmüller, T.; Iversen, L.; Schmidt, M.; Rhodes, C.; Tu, H.-L.; Lin, W.-C.; Groves, J. T. Single Molecule Tracking on Supported Membranes with Arrays of Optical Nanoantennas. *Nano Lett.* **2012**, *12*, 1717−1721.
(26) Tiu, B. D. B.; Pernites, R. B.; Foster, E. L.; Advincula, R. C. Conducting Polymer-Gold Co-Patterned Surfaces via Nanosphere Lithography. *J. Colloid Interface Sci.* **2015**, *459*, 86−96.
(27) Sadakane, M.; Sasaki, K.; Kunioku, H.; Ohtani, B.; Abe, R.; Ueda, W. Preparation of 3-D Ordered Macroporous Tungsten Oxides and Nano-Crystalline Particulate Tungsten Oxides Using a Colloidal Crystal Template Method, and Their Structural Characterization and Application as Photocatalysts Under Visible Light Irradiation. *J. Mater. Chem.* **2010**, *20*, 1811−1818.
(28) Brown, E. C.; Wilke, S. K.; Boyd, D. A.; Goodwin, D. G.; Haile, S. M. Polymer Sphere Lithography for Solid Oxide Fuel Cells: A Route to Functional, Well-Defined Electrode Structures. *J. Mater. Chem.* **2010**, *20*, 2190−2196.
(29) Gao, T.; Wang, B.; Ding, B.; Lee, J.-K.; Leu, P. W. Uniform and Ordered Copper Nanomeshes by Microsphere Lithography for Transparent Electrodes. *Nano Lett.* **2014**, *14*, 2105−2110.
(30) Liu, Y.; Peters, K.; Mandlmeier, B.; Müller, A.; Fominykh, K.; Rathousky, J.; Scheu, C.; Fattakhova-Rohlfing, D. Macroporous Indium Tin Oxide Electrode Layers as Conducting Substrates for Immobilization of Bulky Electroactive Guests. *Electrochim. Acta* **2014**, *140*, 108−115.
(31) Jumabekov, A. N.; Deschler, F.; Böhm, D.; Peter, L. M.; Feldmann, J.; Bein, T. Quantum-Dot-Sensitized Solar Cells with Water-Soluble and Air-Stable PbS Quantum Dots. *J. Phys. Chem. C* **2014**, *118*, 5142−5149.
(32) Jumabekov, A. N.; Della Gaspera, E.; Xu, Z.-Q.; Chesman, A. S. R.; van Embden, J.; Bonke, S. A.; Bao, Q.; Vak, D.; Bach, U. Back-Contacted Hybrid Organic-Inorganic Perovskite Solar Cells. *J. Mater. Chem. C* **2016**, *4*, 3125−3130.
(33) Retsch, M.; Zhou, Z.; Rivera, S.; Kappl, M.; Zhao, X. S.; Jonas, U.; Li, Q. Fabrication of Large-Area, Transferable Colloidal Monolayers Utilizing Self-Assembly at the Air/Water Interface. *Macromol. Chem. Phys.* **2009**, *210*, 230−241.
(34) Rogach, A. L.; Kotov, N. A.; Koktysh, D. S.; Ostrander, J. W.; Ragoisha, G. A. Electrophoretic Deposition of Latex-Based 3D Colloidal Photonic Crystals: A Technique for Rapid Production of High-Quality Opals. *Chem. Mater.* **2000**, *12*, 2721−2726.
(35) Deckman, H. W.; Dunsmuir, J. H. Natural Lithography. *Appl. Phys. Lett.* **1982**, *41*, 377−379.
(36) Aizenberg, J.; Braun, P. V.; Wiltzius, P. Patterned Colloidal Deposition Controlled by Electrostatic and Capillary Forces. *Phys. Rev. Lett.* **2000**, *84*, 2997−3000.
(37) Zheng, H.; Lee, I.; Rubner, M. F.; Hammond, P. T. Two Component Particle Arrays on Patterned Polyelectrolyte Multilayer Templates. *Adv. Mater.* **2002**, *14*, 569−572.
(38) Xia, Y.; Yin, Y.; Lu, Y.; McLellan, J. Template-Assisted Self-Assembly of Spherical Colloids into Complex and Controllable Structures. *Adv. Funct. Mater.* **2003**, *13*, 907−918.
(39) Denkov, N. D.; Velev, O. D.; Kralchevski, P. A.; Ivanov, I. B.; Yoshimura, J. H.; Nagayama, K. Mechanism of Formation of Two-Dimensional Crystals from Latex Particles on Substrates. *Langmuir* **1992**, *8*, 3183−3190.
(40) Rybczynski, J.; Ebels, U.; Giersig, M. Large-Scale, 2D Arrays of Magnetic Nanoparticles. *Colloids Surf., A* **2003**, *219*, 1−6.
(41) Lee, S.-H.; Teshima, K.; Fujisawa, M.; Fujii, S.; Endo, M.; Oishi, S. Fabrication of Highly Ordered, Macroporous $Na_2W_4O_{13}$ Arrays by Spray Pyrolysis Using Polystyrene Colloidal Crystals as Templates. *Phys. Chem. Chem. Phys.* **2009**, *11*, 3628−3633.
(42) Oide, A.; Asoh, H.; Ono, S. Natural Lithography of Si Surfaces Using Localized Anodization and Subsequent Chemical Etching. *Electrochem. Solid-State Lett.* **2005**, *8*, G172−G175.
(43) Zhou, Q.; McIntosh, D. C.; Chen, Y.; Sun, W.; Li, Z.; Campbell, J. C. Nanosphere Natural Lithography Surface Texturing as Anti-Reflective Layer on SiC Photodiodes. *Opt. Express* **2011**, *19*, 23664−23670.
(44) Chen, B.; Zhou, Q.; McIntosh, D. C.; Yuan, J.; Chen, Y.; Sun, W.; Campbell, J. C.; Holmes, A. L., Jr. Natural Lithography Nano-Sphere Texturing as Antireflective Layer on InP-Based pin Photodiodes. *Electron. Lett.* **2012**, *48*, 1340−1341.
(45) Kosmulski, M. The Significance of the Difference in the Point of Zero Charge between Rutile and Anatase. *Adv. Colloid Interface Sci.* **2002**, *99*, 255−264.
(46) Parks, G. A. The Isoelectric Points of Solid Oxides, Solid Hydroxides, and Aqueous Hydroxo Complex Systems. *Chem. Rev.* **1965**, *65*, 177−198.
(47) Tan, Z.-K.; Moghaddam, R. S.; Lai, M. L.; Docampo, P.; Higler, R.; Deschler, F.; Price, M.; Sadhanala, A.; Pazos, L. M.; Credgington, D.; Hanusch, F.; Bein, T.; Snaith, H. J.; Friend, R. H. Bright Light-Emitting Diodes Based on Organometal Halide Perovskite. *Nat. Nanotechnol.* **2014**, *9*, 687−692.
(48) Brochier Salon, M.-C.; Belgacem, M. N. Competition between Hydrolysis and Condensation Reactions of Trialkoxysilanes, as a Function of the Amount of Water and the Nature of the Organic Group. *Colloids Surf., A* **2010**, *366*, 147−154.
(49) Sakai, N.; Tatsuma, T. Photovoltaic Properties of Glutathione-Protected Gold Clusters Adsorbed on TiO_2 Electrodes. *Adv. Mater.* **2010**, *22*, 3185−3188.
(50) Kuo, C.-H.; Chang, H.-Y.; Liu, C.-P.; Lee, S.-H.; You, Y.-W.; Shyue, J.-J. Effect of Surface Chemical Composition on the Surface Potential and Isoelectric Point of Silicon Substrates Modified with Self-Assembled Monolayers. *Phys. Chem. Chem. Phys.* **2011**, *13*, 3649−3653.
(51) Zheng, Y.; Thai, T.; Reineck, P.; Qiu, L.; Guo, Y.; Bach, U. DNA-Directed Self-Assembly of Core-Satellite Plasmonic Nanostructures: A Highly Sensitive and Reproducible Near-IR SERS Sensor. *Adv. Funct. Mater.* **2013**, *23*, 1519−1526.
(52) Shalan, A. E.; Oshikiri, T.; Narra, S.; Elshanawany, M. M.; Ueno, K.; Wu, H.-P.; Nakamura, K.; Shi, X.; Diau, W.-G. E.; Misawa, H. Cobalt Oxide (CoOx) as an Efficient Hole-Extracting Layer for High-Performance Inverted Planar Perovskite Solar Cells. *ACS Appl. Mater. Interfaces* **2016**, *8*, 33592−33600.
(53) Huang, A.; Lei, L.; Yu, Y.; Liu, Y.; Yang, S.; Bao, S.; Cao, X.; Jin, P. Enhanced Electrical Property of Ni-doped CoOx Hole Transport Layer for Inverted Perovskite Solar Cells. *Nanotechnology* **2017**, *28*, 20LT02.

DOI: 10.1021/acsaem.7b00213
ACS Appl. Energy Mater. 2018, 1, 1077−1082